EPJ Web of Conferences **71**, 00009 (2014)
DOI: 10.1051/epjconf/20147100009

Review of recent Heavy Flavour Physics results from the ATLAS experiment

Dario Barberis[1,a]
on behalf of the ATLAS Collaboration

[1] *Università di Genova e INFN, Genova, Italy*

Abstract. Recent ATLAS B-Physics results at 7 TeV centre-of-mass energy at the Large Hadron Collider (LHC) at CERN include the measurements of B^+ production cross-sections and the angular analyses of the decays $B_d^0 \to K^{*0}\mu^+\mu^-$, $B_s^0 \to J/\psi\phi$ and $\Lambda_b^0 \to \Lambda^0 J/\psi$. All measurements done so far are in good agreement with Standard Model predictions.

1 Introduction

The ATLAS experiment [1] at the Large Hadron Collider (LHC) [2] accelerator at CERN recorded an integrated luminosity of 4.9 fb^{-1} of pp collisions at a centre-of-mass energy of 7 TeV in 2011. This dataset has been used to measure several B meson and baryon production and decay properties.

Measurements of the b-hadron production cross-section in proton–proton collisions at the LHC provide further tests of QCD calculations for heavy-quark production at higher centre-of-mass energies and in wider transverse momentum (p_{T}) and rapidity (y) ranges, thanks to the extended coverage and excellent performance of the LHC detectors. In these proceedings we summarise the measurement of the B^+ production cross-section in pp collisions at $\sqrt{s} = 7$ TeV as a function of B^+ transverse momentum and rapidity, using the decay channel $B^+ \to J/\psi K^+ \to \mu^+\mu^- K^+$ [3].

Within the Standard Model the decay $B_d^0 \to K^{*0}\mu^+\mu^-$ occurs via loop diagrams that mediate the transition $b \to s\ell^+\ell^-$ and therefore has a small branching fraction of $(1.06 \pm 0.1) \cdot 10^{-6}$. Angular distributions of the 4-particle final state, as well as the decay amplitudes, are sensitive to physics beyond the Standard Model, mainly as a result of the interference of new diagrams with the Standard Model diagrams [4]. In thee proceedings we summarise the measurement of the lepton forward-backward asymmetry A_{FB} in bins of the di-muon invariant mass q^2 and compare the results to theoretical predictions [5] .

New phenomena beyond the predictions of the Standard Model (SM) may alter CP violation in B-decays. A channel that is expected to be sensitive to new physics contributions is the decay $B_s^0 \to J/\psi\phi$. CP violation in the $B_s^0 \to J/\psi\phi$ decay occurs due to interference between direct decays and decays occurring through $B_s^0 - \overline{B_s^0}$ mixing. The oscillation frequency of B_s^0 meson mixing is characterized by the mass difference Δm_s of the heavy (B_H) and light (B_L) mass eigenstates. The CP-violating phase ϕ_s is defined as the weak phase difference between the $B_s^0 - \overline{B_s^0}$ mixing amplitude and

[a] e-mail: Dario.Barberis@cern.ch

the $b \to c\bar{c}s$ decay amplitude. In the absence of CP violation, the B_H state would correspond exactly to the CP-odd state and the B_L to the CP-even state. In the SM the phase ϕ_s is small and can be related to CKM quark mixing matrix elements via the relation $\phi_s \simeq -2\beta_s$, with $\beta_s = \arg[-(V_{ts}V_{tb}^*)/(V_{cs}V_{cb}^*)]$; a value of $\phi_s \simeq -2\beta_s = -0.0368 \pm 0.0018$ rad is predicted in the SM [6]. Many new physics models predict large ϕ_s values whilst satisfying all existing constraints, including the precisely measured value of Δm_s [7]. Another physical quantity involved in $B_s^0 - \overline{B_s^0}$ mixing is the width difference $\Delta\Gamma_s = \Gamma_L - \Gamma_H$ of B_L and $B_H$which is predicted to be $\Delta\Gamma_s = 0.087 \pm 0.021$ ps^{-1} [8]. Physics beyond the SM is not expected to affect $\Delta\Gamma_s$ as significantly as ϕ_s. Extracting $\Delta\Gamma_s$ from data is nevertheless useful as it allows theoretical predictions to be tested. The ATLAS results on these measurements are published in [9] and summarised here.

The experimental measurement of the parity violating decay asymmetry parameter, α_b, for the weak decay $\Lambda_b^0 \to J/\psi(\mu^+\mu^-)\Lambda^0(p^+\pi^-)$ [10] is also summarised here. Several models have been deployed to predict the value of α_b. One assumption is that the parameter can be extracted by representing the $\Lambda_b^0 \to J/\psi(\mu^+\mu^-)\Lambda^0(p^+\pi^-)$ as a factorized hard scattering coupled with universal hadron distribution amplitudes. In the kinematic domain of the Λ_b^0 produced in the LHC there is a considerable confidence that the hard scattering function can be accurately calculated in perturbative QCD. Models of this type suggest α_b values in the vicinity of -0.2 [11]. Contrary to this prediction, models based of a Heavy Quark Effective Theory (HQET) give a value near 0.8 [12].

2 The ATLAS detector

The ATLAS experiment [1] uses a general-purpose detector consisting of an inner tracker, a calorimeter and a muon spectrometer. ATLAS uses a right-handed coordinate system (x, y, z) with its origin at the nominal interaction point. The z-axis is along the beam pipe, the x-axis points to the centre of the LHC ring and the y-axis points upward. Cylindrical coordinates (r, ϕ) are used in the transverse plane, ϕ being the azimuthal angle around the beam pipe. The pseudorapidity η is defined as $\eta = -\ln[\tan(\theta/2)]$, where θ is the polar angle.

The inner detector (ID) directly surrounds the interaction point; it includes a silicon pixel detector (Pixel), a silicon microstrip detector (SCT) and a transition radiation tracker (TRT), and is embedded in an axial 2 T magnetic field. The ID covers the range $|\eta| < 2.5$ and is enclosed by a calorimeter system containing electromagnetic and hadronic sections.

The calorimeter is surrounded by a large muon spectrometer (MS) inside an air-core toroidal magnet system that contains a combination of monitored drift tubes (MDTs) and cathode strip chambers (CSCs), designed to provide precise position measurements in the bending plane in the range $|\eta| < 2.7$. In addition, resistive plate chambers (RPCs) and thin gap chambers (TGCs) with a coarse position resolution but a fast response time are used primarily to trigger muons in the ranges $|\eta| < 1.05$ and $1.05 < |\eta| < 2.4$, respectively. RPCs and TGCs are also used to provide position measurements in the non-bending plane and to improve pattern recognition and track reconstruction. Momentum measurements in the MS are based on track segments formed in at least two of the three stations of the MDTs and the CSCs.

The ATLAS trigger system [13] has three levels: the hardware-based Level-1 trigger and the two-stage High Level Trigger (HLT), comprising the Level-2 trigger and Event Filter (EF). At Level-1, the muon trigger searches for patterns of hits satisfying different p_{T} thresholds using the RPCs and TGCs. The region-of-interest (RoI) around these Level-1 hit patterns then serves as a seed for the HLT muon reconstruction, in which dedicated algorithms are used to incorporate information from both the MS and the ID, achieving a position and momentum resolution close to that provided by the offline muon reconstruction.

3 B^+ production differential cross sections

This analysis [3] is based on data collected at the LHC during the proton–proton running period in the early 2011 (April–August) with a dimuon trigger that required the presence of at least two opposite sign muon candidates with $p_{\mathrm{T}} > 4$ GeV, an invariant mass compatible with a J/ψ and coming from a common vertex. Selected events are required to have occurred during stable LHC beam conditions and the ID, as well as the MS, must have been fully operational. The collected data correspond to an integrated luminosity of 2.4 fb^{-1} with an uncertainty of 1.8%.

In the analysis two Monte Carlo (MC) samples are used, which simulate respectively the signal $B^{\pm} \to J/\psi\, K^{\pm} \to \mu^+\mu^-\, K^{\pm}$ and the backgrounds from $b\bar{b}$ production, with $b\bar{b} \to J/\psi\, X \to \mu^+\mu^-\, X$, which are relevant for the analysis. Both samples were generated with Pythia 6 using the 2011 ATLAS tune. The response of the ATLAS detector was simulated using Geant4. Additional pp interactions in the same and nearby bunch crossings (pile-up) were included in the simulation.

The differential cross-section for B^+ meson production in pp collisions times branching ratio to the final state is given by

$$\frac{\mathrm{d}^2\sigma(pp \to B^+X)}{\mathrm{d}p_{\mathrm{T}}\mathrm{d}y} \cdot \mathcal{B} = \frac{N^{B^+}}{\mathcal{L} \cdot \Delta p_{\mathrm{T}} \cdot \Delta y}\,, \tag{1}$$

where $\mathcal{B}$ is the total branching ratio of the signal decay, which is $(6.03 \pm 0.21) \times 10^{-5}$, obtained by combining the world-average values of the branching ratios for $B^+ \to J/\psi\, K^+$ and $J/\psi \to \mu^+\mu^-$, N^{B^+} is the number of $B^+ \to J/\psi\, K^+$ signal decays produced, $\mathcal{L}$ is the integrated luminosity of the data sample and Δp_{T}, Δy are the widths of p_{T} and y intervals. Assuming that B^+ and B^- mesons are produced in equal numbers, N^{B^+} is derived from the average yield of the two reconstructed charged states in a (p_{T}, y) interval, after correcting for detector effects and acceptance,

$$N^{B^+} = \frac{1}{A}\frac{N^{B^+}_{\mathrm{reco}}}{\varepsilon^{B^+}} = \frac{1}{A}\frac{N^{B^-}_{\mathrm{reco}}}{\varepsilon^{B^-}} = \frac{1}{A}\frac{N^{B^\pm}_{\mathrm{reco}}}{\varepsilon^{B^+} + \varepsilon^{B^-}}\,, \tag{2}$$

where $N^{B^\pm}_{\mathrm{reco}}$ is the number of reconstructed signal events, obtained from data with a fit to the invariant mass distribution of $B^{\pm}$ candidates, A is the acceptance of the kinematic selection of the final-state particles of the signal decay, obtained from MC simulation, and ε^{B^+}, ε^{B^-} are the reconstruction efficiencies for the $B^{\pm}$ signal decays. The reconstruction efficiencies for B^+ and B^- are obtained from MC simulation, corrected using data-driven methods.

The number of reconstructed $B^{\pm}$ mesons is obtained using a binned maximum likelihood fit to the invariant mass distribution of the selected candidates. The total number of signal $B^{\pm}$ events observed in data in the full p_{T} and y range covered by the analysis, 9 GeV $< p_{\mathrm{T}} <$ 120 GeV and $|y| < 2.25$, before acceptance and efficiency corrections, is about 125600. These events populate four intervals in $|y|$ and eight intervals in p_{T} for the differential cross-section measurement. The acceptance correction, A, has a small dependence on y and ranges from 4% to 85% from the low to the high p_{T} intervals. The efficiency ε^{B^+} has a dependence on both y and p_{T} and ranges from 25% to 40%. The relative difference between the efficiencies for reconstructing B^+ and B^- mesons, $(\varepsilon^{B^+} - \varepsilon^{B^-})/\varepsilon^{B^+}$, has a dependence on p_{T} and ranges from 5% to 2%.

Various sources of systematic uncertainty on the measurement of the B^+ production cross-section are considered. In most intervals, the systematic uncertainty dominates.

Using eq. (1), the differential cross-section for B^+ production times the total branching ratio $\mathcal{B}$ is obtained as a function of p_{T} and y of the B^+ meson and the results are shown in figure 1, averaged over each (p_{T}, y) interval. The double-differential cross-section is integrated over p_{T} to obtain the differential cross-section $\mathrm{d}\sigma/\mathrm{d}y$, or over rapidity to obtain $\mathrm{d}\sigma/\mathrm{d}p_{\mathrm{T}}$, and results are reported in figure 2.

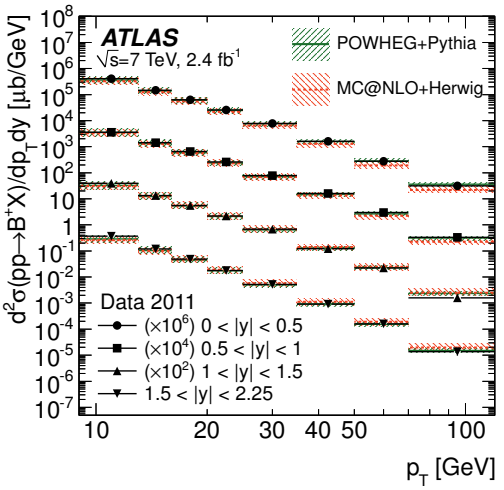

Figure 1. Double-differential cross-section of B^+ production as a function of p_{T} and y, averaged over each (p_{T}, y) interval and quoted at its centre [3]. The data points are compared to NLO predictions from Powheg and MC@NLO. The shaded areas around the theoretical predictions reflect the uncertainty from renormalisation and factorisation scales and the b-quark mass.

Powheg and MC@NLO predictions are compared with the double-differential cross-section measurement in figure 1. The data are in good agreement with Powheg in all rapidity intervals. MC@NLO, however, predicts a lower production cross-section at low p_{T} and a p_{T} spectrum that is softer than the data for $|y| < 1$ and harder than the data for $|y| > 1$.

The FONLL prediction is compared with the measured differential cross-section $\mathrm{d}\sigma/\mathrm{d}p_{\mathrm{T}}$ in figure 2a. In this figure, the results from CMS for B^+ meson production as a function of p_{T}, covering the rapidity range $|y| < 2.4$, are shown for comparison. The FONLL prediction is in good agreement with the data concerning the behaviour in rapidity and p_{T}, within the theoretical uncertainties. All available predictions for $\mathrm{d}\sigma/\mathrm{d}y$ are compared with data in figure 2b. The measured cross-section has a small rapidity dependence and is in agreement with the predictions within their uncertainties. The theoretical uncertainties in all cases are large (~30%) and are similar for the Powheg, MC@NLO and FONLL predictions.

The integrated B^+ production cross-section in the kinematic range 9 GeV $< p_{\mathrm{T}} <$ 120 GeV and $|y| < 2.25$ is:

$$\sigma(pp \to B^+X) = 10.6 \pm 0.3\ (\mathrm{stat.}) \pm 0.7\ (\mathrm{syst.}) \pm 0.2\ (\mathrm{lumi.}) \pm 0.4\ (\mathcal{B})\ \mu\mathrm{b}.$$

The FONLL prediction, with its theoretical uncertainty from the renormalisation and factorisation scale and the b-quark mass, is:

$$\sigma(pp \to bX) \cdot f_{\bar{b}\to B^+} = 8.6^{+3.0}_{-1.9}\ (\mathrm{scale}) \pm 0.6\ (m_b)\ \mu\mathrm{b}\ ,$$

where $f_{\bar{b}\to B^+} = (40.1 \pm 0.8)\%$ is the world-average value for the hadronisation fraction. The corresponding predictions of Powheg and MC@NLO are 9.4 μb and 8.8 μb, respectively, with theoretical uncertainties similar to the FONLL prediction.

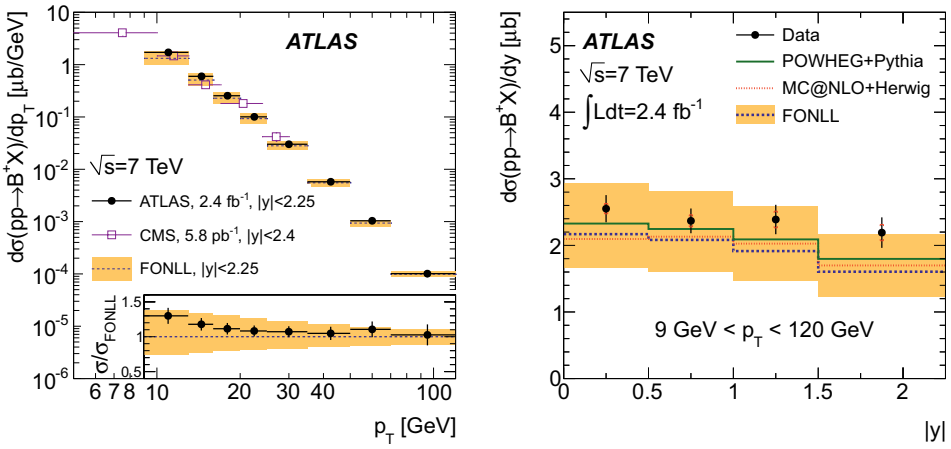

Figure 2. (a) Differential cross-section of B^+ production vs p_{T}, integrated over rapidity [3]. The solid circle points with error bars correspond to the differential cross-section measurement of ATLAS with total uncertainty (statistical and systematic) in the rapidity range $|y| < 2.25$, averaged over each p_{T} interval and quoted at its centre. For comparison, data points from CMS are also shown, for a measurement covering $p_{\mathrm{T}} < 30$ GeV and $|y| < 2.4$. Predictions of the FONLL calculation for b-quark production are also compared with the data, assuming a hadronisation fraction of $f_{\bar{b}\to B^+}$ of $(40.1 \pm 0.8)\%$ to fix the overall scale. Also shown is the ratio of the measured cross-section to the predictions of the FONLL calculation ($\sigma/\sigma_{\mathrm{FONLL}}$). The upper and lower uncertainty limits on the prediction were obtained considering scale and b-quark mass variations. (b) Differential cross-section of B^+ production vs rapidity, integrated over p_{T}. Points with error bars correspond to the differential cross-section measurement with total uncertainty (lines on the error bars indicate the statistical component) in the p_{T} range 9 GeV $< p_{\mathrm{T}} <$ 120 GeV, averaged over each rapidity interval and quoted at its centre. POWHEG, MC@NLO and FONLL predictions are also given for comparison. The relevant uncertainties of the predictions of POWHEG and MC@NLO are of the same order as for FONLL and are not shown.

The results are reported for B^+ meson production, but are derived from both charged states, taking into account the different reconstruction efficiencies for B^+ and B^-, under the assumption that in the phase space accessible by this measurement the B^+ and B^- production cross-sections are equal; this assumption is in agreement with the predictions of NLO Monte Carlo generators and is also valid within the precision of the measurement.

4 Angular analysis of the decay $B^0_d \to K^{*0}\mu^+\mu^-$

The decay $B^0_d \to K^{*0}\mu^+\mu^-$ with $K^{*0} \to K^+\pi^-$ is described by four kinematic variables: one is the invariant mass q^2 of the di-muon system and the other three are angles describing the geometrical configuration of the final state as shown in figure 3: θ_L is the angle between the μ^+ and the direction opposite to the B^0_d in the di-muon rest frame, θ_K is the angle between the K^+ and the direction opposite to the B^0_d in the K^{*0} rest frame, and ϕ is the angle between the plane defined by the two muons and the plane defined by the kaon-pion system in the B^0_d rest frame. In the case of the $\overline{B}^0_d$ the angles θ_L and θ_K are defined with respect to the μ^- and the K^-, respectively. When the amount of data is insufficient to study the 4-differential decay rate, the differential decay rate is projected from the four kinematic variables into the 2-dimensional distributions $\mathrm{d}^2\Gamma/\mathrm{d}q^2\mathrm{d}\cos\theta_L$ and $\mathrm{d}^2\Gamma/\mathrm{d}q^2\mathrm{d}\cos\theta_K$ by

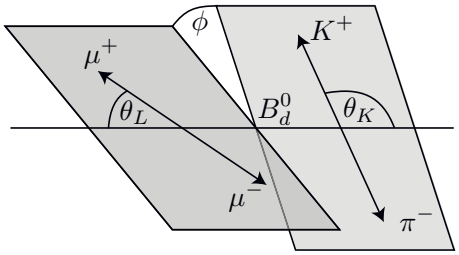

Figure 3. Definition of the kinematic angles in the decay $B_d^0 \to K^{*0}\mu^+\mu^-$ [5].

integrating over the two other variables. These distributions are binned in intervals of q^2, and the values of the K^{*0} longitudinal polarisation fraction F_L and of the lepton forward-backward asymmetry A_{FB} are extracted, averaged in the q^2 bins [5] .

This analysis uses 4.9 fb^{-1}of data from pp-collisions at $\sqrt{s} = 7$ TeV collected in 2011. Data are only used if both the ID and MS subsystems were fully operational and the LHC proton beams were stable.

Monte Carlo events have been generated with Pythia for the signal decay channel $B_d^0 \to K^{*0}\mu^+\mu^-$, the resonant background decay channel $B_d^0 \to K^{*0}J/\psi$ and generic $b\bar{b}$ and $c\bar{c}$ production with two muons in the final state. Furthermore a sample of Drell-Yan events has been generated.

Given the increasing luminosity during the data taking period, several single-muon and di-muon triggers are used to select the events, with different transverse momentum thresholds. The main triggers select di-muon events requiring both muons to have $p_{\mathrm{T}}(\mu) > 4$ GeV, or alternatively $p_{\mathrm{T}}(\mu_1) > 6$ GeV and $p_{\mathrm{T}}(\mu_2) > 4$ GeV. The high-rate triggers were prescaled at higher luminosity. Monte Carlo studies show, that the trigger efficiency relative to the offline selection is 96 %.

Each event has to contain at least one reconstructed primary vertex with a minimum of four associated ID tracks with $p_{\mathrm{T}} > 0.5$ GeV, and is required to have at least two muon candidates with opposite charge. The $K^{*0}/\overline{K}^{*0} \to K^{\pm}\pi^{\mp}$ candidates are reconstructed from all pairs of oppositely charged particles with $p_{\mathrm{T}} > 0.5$ GeV and $|\eta| < 2.5$ that are not identified as muons. For the reconstruction of $B_d^0 \to K^{*0}\mu^+\mu^-$ candidates, all combinations of di-muon pairs and $K^{*0} \to K^+\pi^-$ candidates are considered. Using these requirements, a total of approximately $64 \cdot 10^6$ candidates are selected in the invariant mass region of 4600 MeV $< m(K\pi\mu\mu) <$ 5900 MeV. In order to avoid background from events containing J/ψ and $\psi(2S)$, regions in di-muon mass are excluded which cover 3σ around the $J/\psi \to \mu^+\mu^-$ and $\psi(2S) \to \mu^+\mu^-$ decay peaks. After removing those events, a total of approximately $23 \cdot 10^6$ candidates are selected.

We select events in the mass region 4600 MeV $< m(K\pi\mu\mu) <$ 5900 MeV and are left with 4 466 candidates in the full q^2 range, after the optimised selection. The full q^2 range is defined as the three continuous intervals obtained by removing the J/ψ and $\psi(2S)$ regions as discussed earlier from the interval 1.00 GeV$^2 < q^2 <$ 19.00 GeV^2.

The values for A_{FB} and F_L are extracted by performing a sequential unbinned maximum likelihood fit, where in a first step the invariant $K\pi\mu\mu$ mass distribution is fitted, then the resulting parameters are fixed, and in a second step - where the signal and background yields are fixed by the previous fit - the angular distributions are fitted.

The differential decay rate of $B_d^0 \to K^{*0}\mu^+\mu^-$ is parametrized by the invariant di-muon mass q^2 and the three helicity angles θ_L, θ_K and ϕ in the rest frame of the four particle final state. At a given

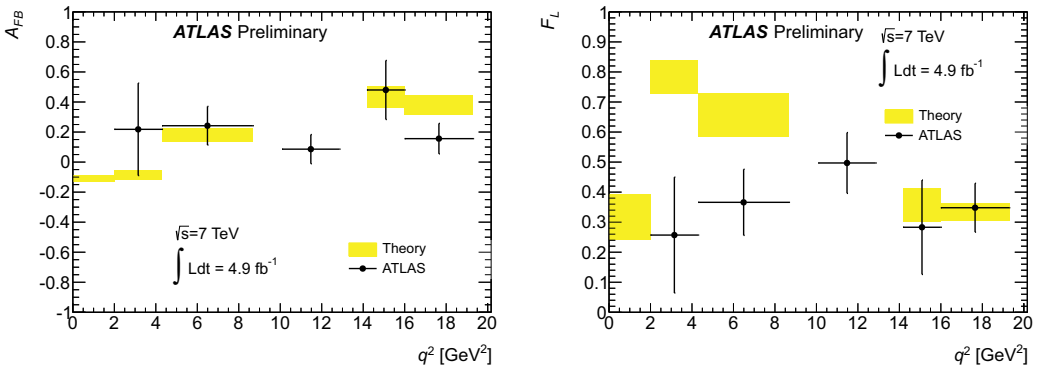

Figure 4. (a) Forward-backward asymmetry A_{FB} and (b) fraction of longitudinally polarised K^{*0} mesons, F_L, including statistical and systematic uncertainties, compared to theoretical predictions calculated for the limits of small and large values of q^2 including theoretical uncertainties [5] .

q^2 the integration of the differential decay rate over θ_K and ϕ gives

$$\frac{1}{\Gamma}\frac{\mathrm{d}^2\Gamma}{\mathrm{d}q^2\mathrm{d}\cos\theta_L} = \frac{3}{4}F_L(q^2)\left(1-\cos^2\theta_L\right) + \frac{3}{8}\left(1-F_L(q^2)\right)\left(1+\cos^2\theta_L\right) + A_{FB}(q^2)\cos\theta_L \tag{3}$$

and the integration of the differential decay rate over θ_L and ϕ yields

$$\frac{1}{\Gamma}\frac{\mathrm{d}^2\Gamma}{\mathrm{d}q^2\mathrm{d}\cos\theta_K} = \frac{3}{2}F_L(q^2)\cos^2\theta_K + \frac{3}{4}\left(1-F_L(q^2)\right)\left(1-\cos^2\theta_K\right). \tag{4}$$

Fixing the parameters obtained in the invariant mass fit, the likelihood function for the angular distributions is written as

$$\mathcal{L} = \prod_{i=1}^{N}[N_{\mathrm{sig}}^{fix}\cdot\mathcal{M}_{\mathrm{sig}}(m_i,\delta_{m_i}|\mathrm{fixed})\cdot\mathcal{A}_{L,\mathrm{sig}}(\cos\theta_{L,i})\cdot\alpha_L(\cos\theta_{L,i})\cdot\mathcal{A}_{K,\mathrm{sig}}(\cos\theta_{K,i})\cdot\alpha_K(\cos\theta_{K,i}) + N_{\mathrm{bckg}}^{fix}\cdot\mathcal{M}_{\mathrm{bckg}}(m_i|\mathrm{fixed})\cdot\mathcal{A}_{L,\mathrm{bckg}}(\cos\theta_{L,i})\cdot\mathcal{A}_{K,\mathrm{bckg}}(\cos\theta_{K,i})], \tag{5}$$

where the $\mathcal{A}$'s denote the probability density functions of the angular distributions of $\cos\theta_K$ and $\cos\theta_L$ for the signal and the background. The angular distributions of the signal are given by Equations (3) and (4). To take into account angular detector efficiencies due to trigger, event reconstruction, detector effects and the selection cuts, the angular signal distributions are weighted by acceptance maps α_K and α_L, determined for $\cos\theta_K$ and $\cos\theta_L$, respectively.

The parameters A_{FB} and F_L are extracted in five q^2 bins from 2.00 GeV^2 to 19.00 GeV^2 and in the wider bin 1.00 GeV^2 $< q^2 <$ 6.00 GeV^2. The final results of the unbinned maximum likelihood fit including statistical and systematic uncertainties are summarised in Table 1. In figure 4 the results for A_{FB} and F_L are compared to Standard Model expectations. The theoretical expectations have been calculated for the limits of small and large vector meson energy; no expectation is given for the central q^2 region.

Table 1. Summary of the fit results for the different bins of q^2. Number of signal events N_{sig} from the mass fit and its statistical uncertainty, forward backward asymmetry A_{FB} and longitudinal polarisation F_L for different bins in q^2 including statistical and systematic uncertainties [5] .

q^2 range (GeV^2)	N_{sig}	A_{FB}	F_L
$2.00 < q^2 < 4.30$	19 ± 8	$0.22 \pm 0.28 \pm 0.14$	$0.26 \pm 0.18 \pm 0.06$
$4.30 < q^2 < 8.68$	88 ± 17	$0.24 \pm 0.13 \pm 0.01$	$0.37 \pm 0.11 \pm 0.02$
$10.09 < q^2 < 12.86$	138 ± 31	$0.09 \pm 0.09 \pm 0.03$	$0.50 \pm 0.09 \pm 0.04$
$14.18 < q^2 < 16.00$	32 ± 14	$0.48 \pm 0.19 \pm 0.05$	$0.28 \pm 0.16 \pm 0.03$
$16.00 < q^2 < 19.00$	149 ± 24	$0.16 \pm 0.10 \pm 0.03$	$0.35 \pm 0.08 \pm 0.02$
$1.00 < q^2 < 6.00$	42 ± 11	$0.07 \pm 0.20 \pm 0.07$	$0.18 \pm 0.15 \pm 0.03$

5 Flavour-tagged time dependent angular analysis of the $B_s^0 \to J/\psi\phi$ decay

The data used for this analysis [9] were collected during a period of rising instantaneous luminosity at the LHC, and the trigger conditions varied over this time. The triggers used to select events for this analysis are based on identification of a $J/\psi \to \mu^+\mu^-$ decay, with either a 4 GeV p_{T} threshold for each muon or an asymmetric configuration that applies a p_{T} threshold beyond 4 GeV p_{T} to one of the muons and accepting the second muon with p_{T} as low as 2 GeV.

Monte Carlo simulation is used to study the detector response, estimate backgrounds and model systematic effects. For this study, 12 million simulated $B_s^0 \to J/\psi\phi$ events were generated using Pythia tuned with recent ATLAS data. No p_{T} cuts were applied at the generator level. In order to take into account the varying trigger configurations during data-taking, the MC events were weighted to have the same trigger composition as the collected collision data. Additional samples of the background decay $B_d^0 \to J/\psi K^{0*}$ as well as the more general $bb \to J/\psi X$ and $pp \to J/\psi X$ backgrounds were also simulated using Pythia.

Events passing the trigger and the data quality selections are required to pass the following additional criteria: the event must contain at least one reconstructed primary vertex built from at least four ID tracks and at least one pair of oppositely charged muon candidates. The candidates for $\phi \to K^+K^-$ are reconstructed from all pairs of oppositely charged particles with $p_{\mathrm{T}} > 0.5$ GeV and $|\eta| < 2.5$ that are not identified as muons. Candidates for $B_s^0 \to J/\psi(\mu^+\mu^-)\phi(K^+K^-)$ are sought by fitting the tracks for each combination of $J/\psi \to \mu^+\mu^-$ and $\phi \to K^+K^-$ to a common vertex. In total 131k B_s^0 candidates are collected within a mass range of $5.15 < m(B_s^0) < 5.65$ GeV used in the fit.

The determination of the initial flavour of neutral B-mesons can be inferred using information from the other B-meson that is typically produced from the other b quark in the event, referred to as the Opposite-Side Tagging (OST). To study and calibrate the OST methods, the decays of $B^\pm \to J/\psi K^\pm$ can be used, where flavour of the charge of the B-meson at production is provided by the kaon charge. Events from the entire 2011 run period satisfying the same data quality selections as previously described are used.

An unbinned maximum likelihood fit is performed on the selected events to extract the parameters of the $B_s^0 \to J/\psi(\mu^+\mu^-)\phi(K^+K^-)$ decay. The fit uses information about the reconstructed mass m, the measured proper decay time t, the measured mass and proper decay time uncertainties σ_m and σ_t, the tag probability, and the transversity angles Ω of each $B_s^0 \to J/\psi\phi$ decay candidate. There are three transversity angles; $\Omega = (\theta_T, \psi_T, \phi_T)$, which are defined in the rest frames of the final-state particles.

The x-axis is determined by the direction of the ϕ meson in the J/ψ rest frame, the K^+K^- system defines the xy plane, where $p_y(K^+) > 0$. The three angles are defined:

- θ_T, the angle between $p(\mu^+)$ and the xy plane, in the J/ψ meson rest frame
- ϕ_T, the angle between the x-axis and $p_{xy}(\mu^+)$, the projection of the μ^+ momentum in the xy plane, in the J/ψ meson rest frame
- ψ_T, the angle between $p(K^+)$ and $-p(J/\psi)$ in the ϕ meson rest frame

The likelihood function is defined as a combination of the signal and background probability density functions as follows:

$$\ln \mathcal{L} = \sum_{i=1}^{N} \{w_i \cdot \ln(f_s \cdot \mathcal{F}_s(m_i, t_i, \Omega_i) + f_s \cdot f_{B^0} \cdot \mathcal{F}_{B^0}(m_i, t_i, \Omega_i) + (1 - f_s \cdot (1 + f_{B^0}))\mathcal{F}_{\text{bkg}}(m_i, t_i, \Omega_i))\} \quad (6)$$

where N is the number of selected candidates, w_i is a weighting factor to account for the trigger efficiency, f_s is the fraction of signal candidates, f_{B^0} is the fraction of peaking B^0 meson background events calculated relative to the number of signal events; this parameter is fixed in the likelihood fit. The mass m_i, the proper decay time t_i and the decay angles Ω_i are the values measured from the data for each event i. $\mathcal{F}_s$, $\mathcal{F}_{B^0}$ and $\mathcal{F}_{\text{bkg}}$ are the probability density functions (pdf) modelling the signal, the specific B^0 background and the other background distributions, respectively.

The full simultaneous maximum likelihood fit contains 25 free parameters. This includes the nine physics parameters: $\Delta\Gamma_s$, ϕ_s, Γ_s, $|A_0(0)|^2$, $|A_\parallel(0)|^2$, $\delta_\parallel$, $\delta_\perp$, $|A_S|^2$ and δ_S. The other parameters in the likelihood function are the B_s^0 signal fraction f_s, the parameters describing the $J/\psi\phi$ mass distribution, the parameters describing the B_s^0 meson decay time plus angular distributions of background events, the parameters used to describe the estimated decay time uncertainty distributions for signal and background events, and scale factors between the estimated decay time and mass uncertainties and their true uncertainties. In addition to this there are also 82 nuisance parameters describing the background and acceptance functions that are fixed at the time of the fit.

The number of signal B_s^0 meson candidates extracted from the fits is 22670 ± 150. The results for the measured physics parameters of the simultaneous unbinned maximum likelihood fit are given in Table 2.

Table 2. Fitted values for the physical parameters along with their statistical and systematic uncertainties [9].

Parameter	Value	Statistical uncertainty	Systematic uncertainty
ϕ_s(rad)	0.12	0.25	0.05
$\Delta\Gamma_s(\text{ps}^{-1})$	0.053	0.021	0.009
$\Gamma_s(\text{ps}^{-1})$	0.677	0.007	0.003
$\lvert A_\parallel(0)\rvert^2$	0.220	0.008	0.009
$\lvert A_0(0)\rvert^2$	0.529	0.006	0.011
$\lvert A_S\rvert^2$	0.024	0.014	0.028
$\delta_\perp$	3.89	0.47	0.13
$\delta_\parallel$	[3.04-3.23]		0.09
$\delta_\perp - \delta_S$	[3.02-3.25]		0.04

Systematic uncertainties are assigned by considering several effects that are not accounted for in the likelihood fit: Inner Detector alignment, angular acceptance method, trigger efficiency, fit model, signal and background mass model, resolution model, background lifetime and background angles model, B_d contribution, tagging uncertainties. For each variable, the total systematic error is obtained adding in quadrature the different contributions.

The pdf describing the $B_s^0 \to J/\psi\phi$ decay is invariant under the following simultaneous transformations:

$$\{\phi_s, \Delta\Gamma, \delta_\perp, \delta_\parallel\} \to (\pi - \phi_s, -\Delta\Gamma, \pi - \delta_\perp, 2\pi - \delta_\parallel).$$

$\Delta\Gamma_s$ has been determined to be positive, therefore there is a unique solution. Uncertainties on individual parameters have been studied in details in likelihood scans. Figure 5 shows the likelihood contours in the ϕ_s - $\Delta\Gamma_s$ plane.

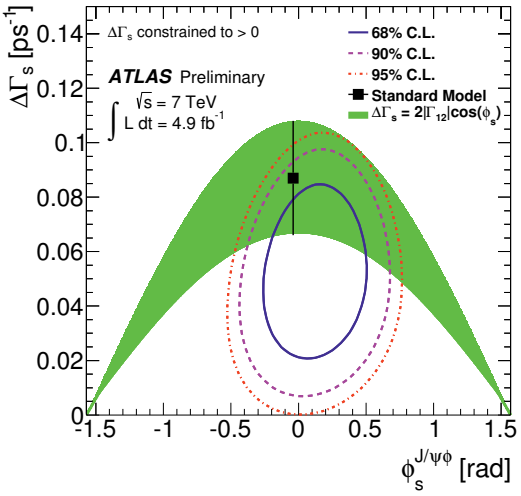

Figure 5. Likelihood contours in ϕ_s - $\Delta\Gamma_s$ plane. The blue and red contours show the 68% and 95% likelihood contours, respectively (statistical errors only). The green band is the theoretical prediction of mixing- induced CP violation [9].

The behaviour of the amplitudes around their fitted values is as expected, however the strong phases are more complicated. The behaviour of $\delta_\perp$ appears gaussian and therefore it is reasonable to quote $\delta_\perp = 3.89 \pm 0.47(stat)$ rad. For $\delta_\perp - \delta_S$ the likelihood scan shows a minimum close to π, however it is insensitive over the rest of the scan at the level of 4.3σ. Therefore the measured value of the difference $\delta_\perp - \delta_S$ is only given as 1σ confidence interval [3.02-3.25] rad. $\delta_\parallel$ shows normal gaussian behaviour around the minimum however the systematic pull plots show unusual behaviour so it is also given in the form of a 1σ confidence interval [3.04-3.23] rad.

6 Parity violating asymmetry parameter α_b and helicity amplitudes for the decay $\Lambda_b^0 \to J/\psi\Lambda^0$

Due to the parity conservation in the strong interaction, strongly-produced Λ_b^0 can only be polarized in a direction $\hat{n}$ which is perpendicular to the Λ_b^0 momentum. The unit vector $\hat{n}$ is chosen to point in

the direction of a cross-product of the beam direction and the Λ_b^0 momentum. There is an ambiguity in choice of the beam direction, since LHC is a pp collider. This analysis uses the positive z-axis direction of the ATLAS coordinate system for the Λ_b^0 candidates and the negative z-axis for $\bar{\Lambda}_b^0$ (to preserve symmetry between Λ^0 and $\bar{\Lambda}^0$ given by the orientation of the ATLAS magnetic field). The Λ_b^0 decay, as well as the subsequent decays of Λ^0 and J/ψ, are 2-body decays, and therefore each of them can be parametrized by a polar and azimuthal angle in their respective rest frames. A definition of the decay angles is shown in figure 6.

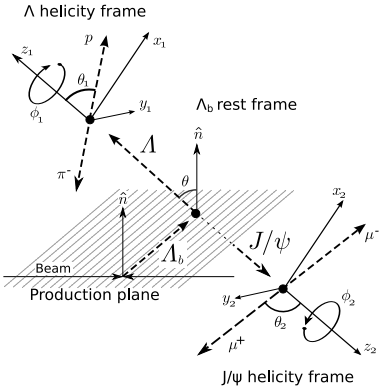

Figure 6. Definition of the decay angles. The angle θ is the polar angle of the Λ^0 momentum measured from the normal direction $\hat{n}$ in the Λ_b^0 rest frame. The angles θ_1 and ϕ_1 are the polar and azimuthal angles of the proton in the Λ^0 rest frame with respect to the Λ^0 direction in the Λ_b^0 rest frame. Similarly, θ_2 and ϕ_2 are polar and azimuthal angles of μ^+ in the J/ψ rest frame with respect to the J/ψ direction in the Λ_b^0 rest frame. The azimuthal angles, ϕ_1 and ϕ_2, are measured in the Λ^0 and J/ψ rest frame right-handed coordinate systems, (x_1, y_1, z_1) and (x_2, y_2, z_2), respectively. The $z_{1,2}$-axes are aligned with the direction of Λ^0 and J/ψ, respectively, and the $x_{1,2}$-axes lie in the plane containing $\hat{n}$ and the Λ^0 or J/ψ momenta. With this definition, the angle $\phi_1 + \phi_2$ is actually the angle between the Λ^0 and J/ψ decay planes [10].

Taking λ_Λ and $\lambda_{J/\psi}$ to represent the helicity of Λ^0 and J/ψ, the considered decay can be described by four helicity amplitudes $A(\lambda_\Lambda, \lambda_{J/\psi})$: $a_+ \equiv A(1/2, 0)$, $a_- \equiv A(-1/2, 0)$, $b_+ \equiv A(-1/2, -1)$, $b_- \equiv A(1/2, 1)$, which should be normalized to unity:

$$|a_+|^2 + |a_-|^2 + |b_+|^2 + |b_-|^2 = 1. \tag{7}$$

The full angular pdf of the decay angles collection $\Omega = (\theta, \phi, \theta_1, \phi_1, \theta_2, \phi_2)$ is:

$$w(\Omega, \vec{A}, P) = \frac{1}{(4\pi)^3} \sum_{i=0}^{19} f_{1i}(\vec{A}) f_{2i}(P, \alpha_\Lambda) F_i(\Omega), \tag{8}$$

where $f_{1i}(\vec{A})$ are bilinear combinations of the helicity amplitudes, $\vec{A} \equiv (a_+, a_-, b_+, b_-)$, f_{2i} is one of the following expressions: $P\alpha_\Lambda$, P, α_Λ or 1, with α_Λ being the decay asymmetry parameter for the decay $\Lambda^0 \to p\pi^-$, and P is the Λ_b^0 polarization. The value of α_Λ is known with high precision, $\alpha_\Lambda = 0.642 \pm 0.013$, and $\alpha_{\bar{\Lambda}} = -0.71 \pm 0.08$ for $\bar{\Lambda}^0 \to p^-\pi^+$. Since there is no evidence of CP violation in Λ^0 and $\bar{\Lambda}^0$ decay and the parameter for Λ^0 is more precisely determined, the value of -0.642 ± 0.013 is used for $\bar{\Lambda}^0$ in this analysis. The minus sign is required by CP conservation. The

$F_i(\Omega)$ are orthogonal functions of the decay angles. The concrete forms of the $f_{1i}(\vec{A})$ and $F_i(\Omega)$ functions are given in [10].

If CP is conserved, the pdf's of Λ_b^0 and $\bar{\Lambda}_b^0$ decay have exactly the same form. Therefore, assuming CP conservation, the Λ_b^0 and $\bar{\Lambda}_b^0$ samples are combined to measure the decay asymmetry parameter α_b and the helicity amplitudes with better precision. The α_b parameter is related to the helicity amplitudes as follows:

$$\alpha_\mathrm{b} = |a_+|^2 - |a_-|^2 + |b_+|^2 - |b_-|^2 \tag{9}$$

There are nine unknown parameters with a real value in the pdf: four complex helicity amplitudes, $a_+ = |a_+|e^{i\rho_+}$, $a_- = |a_-|e^{i\rho_-}$, $b_+ = |b_+|e^{i\omega_+}$, $b_- = |b_-|e^{i\omega_-}$, each with a magnitude and a phase, and polarization P. However, only six out of these eight helicity amplitude parameters are independent, taking into account the normalization constraint and the arbitrariness of the common phase, due to which only the differences between the four phases are relevant. The following five parameters are chosen to define the model:

$$\begin{aligned}
\alpha_\mathrm{b} &= |a_+|^2 - |a_-|^2 + |b_+|^2 - |b_-|^2 \\
k_0 &= \frac{|a_+|}{\sqrt{|a_+|^2 + |b_+|^2}} \\
k_1 &= \frac{|b_-|}{\sqrt{|a_-|^2 + |b_-|^2}} \\
\Delta_+ &= \rho_+ - \omega_+ \\
\Delta_- &= \rho_- - \omega_-
\end{aligned} \tag{10}$$

This analysis [10] uses 7 TeV collision data collected in 2011 using single-muon and J/ψ triggers. The corresponding integrated luminosity is 4.6 fb^{-1}. Since the rate from the low-p_T muon triggers was too high, prescale factors were applied to reduce the output rate. The transverse momentum threshold for single muon triggers is 18 GeV. The J/ψ triggers are di-muon triggers which in addition require that the muons have an opposite charge, come from a common vertex and and that the di-muon mass is in the interval 2.5 GeV $< m_{\mu\mu} <$ 4.3 GeV. The majority of the sample was collected by the J/ψ trigger with a p_T threshold of 4 GeV applied to both muons, the lowest p_T-threshold trigger unprescaled in the 2011 data taking period. Altogether, the used triggers collected muons with p_T spectrum peaking at about 5 GeV with minimum p_T above 2.5 GeV.

A Monte Carlo sample of 5 million signal events is used to study the effect of the efficiency and acceptance of the detector. The sample is generated using the Pythia6.4 MC generator and the events are filtered such that each event contains a signal decay with the muons having transverse momenta above 2.5 GeV. In addition to the Λ_b^0 MC samples, $B_d^0 \to J/\psi(\mu^+\mu^-)K_S^0(\pi^+\pi^-)$ and $b\bar{b} \to J/\psi + X$ MC samples are also generated using Pythia to optimize the selection cuts and understand the sources of background.

The decay $\Lambda_b^0 \to J/\psi(\mu^+\mu^-)\Lambda^0(p^+\pi^-)$ has a cascade topology. The di-muon candidates are accepted if the J/ψ vertex-refitted invariant mass lies in the range 2.8 GeV $< m_{\mu\mu} <$ 3.4 GeV. The di-hadron candidates are accepted if the invariant mass is in the range 1.08 GeV $< m_{p\pi} <$ 1.15 GeV. The masses of a proton and a pion are assigned to the tracks when the invariant mass is calculated; $p\pi^-$ and $\bar{p}\pi^+$ combinations are considered so that both Λ^0 and $\bar{\Lambda}^0$ candidates are accepted. The muon and hadronic track pairs are then refitted with the constraint of a $\Lambda_b^0 \to J/\psi(\mu^+\mu^-)\Lambda^0(p^+\pi^-)$ topology. After the selection, there are in total 1548 Λ_b^0 and $\bar{\Lambda}_b^0$ candidates (including background) in the signal region.

The helicity amplitudes and the α_b parameter are extracted from the expected value of each of the F_i variables in the pdf, as described in [10]. As the combinatorial background changes linearly

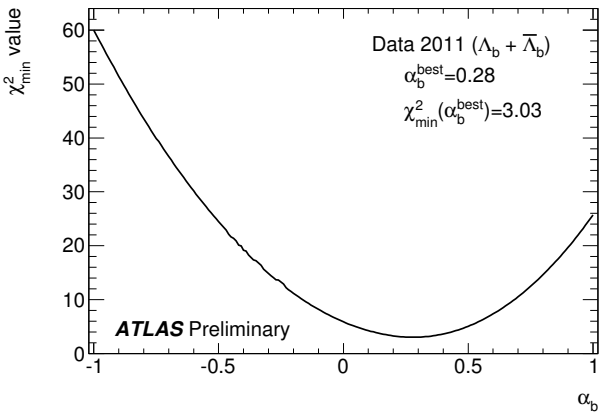

Figure 7. The conditional $\chi^2_{\rm min}$ as a function of $\alpha_{\rm b}$ [10].

with the Λ_b^0 mass, its contribution to the measured $\langle F_i \rangle$ values can be estimated using events in the invariant mass sidebands. Two mass windows define the sidebands: $5400 < m_{J/\psi\Lambda^0} < 5520$ MeV is chosen as the left sideband and $5720 < m_{J/\psi\Lambda^0} < 5840$ MeV as the right one. These two sidebands have almost the same distance to the mass of Λ_b^0 and have the same size as the signal mass window, so the background contribution to the $\langle F_i \rangle$ values in the central region can be simply estimated as an average of the values in the two sidebands. The estimated background contribution is subtracted from the measured value of $\langle F_i \rangle$.

The χ^2 fit is performed and the values obtained from the fit are

$$\begin{aligned} \alpha_{\rm b} &= 0.28 \pm 0.16, \\ k_0 &= 0.22^{+0.14}_{-0.57}, \\ k_1 &= 0.13^{+0.20}_{-0.47}. \end{aligned} \tag{11}$$

The uncertainty of the parameters are calculated by finding the range that satisfies $\chi^2 - \chi^2_{\rm min} < 1$. With the current data statistics, values of the relative phases, Δ_+ and Δ_-, cannot be determined with sufficient precision and are consistent with the entire allowed range, $[-\pi, \pi]$. However, it is found that their large uncertainties have a small effect on the determination of $\alpha_{\rm b}$, k_0 and k_1. Figure 7 shows the $\chi^2_{\rm min}$ as a function of the assumed $\alpha_{\rm b}$ parameter, under the condition that $\alpha_{\rm b}$ is fixed in the fit. The minimum of this conditional $\chi^2_{\rm min}$ curve gives the central value of $\alpha_{\rm b}$, $\alpha_{\rm b}^{best}$, and the corresponding χ^2 value is 3.03.

The absolute values of the helicity amplitudes were calculated from the fitted parameters and the statistical uncertainties were calculated using error propagation:

$$\begin{aligned} |a_+| &= 0.17^{+0.12}_{-0.17}, \\ |a_-| &= 0.59^{+0.06}_{-0.07}, \\ |b_+| &= 0.78^{+0.04}_{-0.05}, \\ |b_-| &= 0.08^{+0.13}_{-0.08}. \end{aligned} \tag{12}$$

It is worth noting that the Λ_b^0 decay has large amplitudes $|a_-|$ and $|b_+|$, which means the negative-helicity states for Λ^0 are preferred. The Λ^0 and J/ψ from Λ_b^0 decay are highly polarized. Combining

in quadrature the statistical and systematic uncertainties, the observed value of α_b is consistent with the recent measurement of LHCb at the level of one standard deviation, however, it is not consistent with the expectation from pQCD [$\alpha_b = -(0.14 \sim 0.18)$], and HQET ($\alpha_b = 0.78$) at a level of about 2.5 and 2.9 standard deviation, respectively. A more precise determination of α_b and of the decay amplitudes will be possible with the sample of data collected by the ATLAS experiment in 2012.

7 Conclusions

Thanks to its good inner tracking and muon detector systems, as well as the large acceptance triggers, ATLAS is able to contribute significant results in heavy flavour physics. Recent analyses, still based on 2011 data, measured the differential B^+ production cross-sections and the angular distributions in the decays $B_d^0 \to K^{*0}\mu^+\mu^-$, $B_s^0 \to J/\psi\phi$ and $\Lambda_b^0 \to J/\psi(\mu^+\mu^-)\Lambda^0(p^+\pi^-)$. All measurements done so far are in good agreement with Standard Model predictions, or at least, don't show any significant deviation from the predictions. Additional statistics from the 2012 run will soon reduce statistical errors on all results.

References

[1] The ATLAS Collaboration, JINST 3, S08003 (2008), doi:10.1088/1748-0221/3/08/S08003

[2] L. Evans and P. Bryant, JINST 3, S08001 (2008), doi:10.1088/1748-0221/3/08/S08001

[3] The ATLAS Collaboration, JHEP 10 (2013) 042, doi:10.1007/JHEP10(2013)042

[4] T. Feldmann and J. Matias, JHEP 0301 (2003) 074, arXiv:hep-ph/0212158

[5] The ATLAS Collaboration, ATLAS-CONF-2013-038, https://cds.cern.ch/record/1537961/files/ATLAS-CONF-2013-038.pdf

[6] UTfit Collaboration, M. Bona et al., Phys.Rev.Lett. 97 (2006) 151803, arXiv:hep-ph/0605213

[7] CDF Collaboration, A. Abulencia et al., Phys.Rev.Lett. 97 (2006) 242003, arXiv:hep-ex/0609040

[8] A. Lenz and U. Nierste, JHEP 0706 (2007) 072, arXiv:hep-ph/0612167

[9] The ATLAS Collaboration, ATLAS-CONF-2013-039, https://cds.cern.ch/record/1541823/files/ATLAS-CONF-2013-039.pdf

[10] The ATLAS Collaboration, ATLAS-CONF-2013-071, https://cds.cern.ch/record/1562908/files/ATLAS-CONF-2013-071.pdf

[11] C.-H. Chou, H.-H. Shih, S.-C. Lee, and H.-n. Li, Phys.Rev. D65 (2002) 074030, arXiv:hep-ph/0112145

[12] O. Leitner, Z. Ajaltouni, and E. Conte, Nucl.Phys. A755 (2005) 435–438, arXiv:hep-ph/0412131
Z. Ajaltouni, E. Conte, and O. Leitner, Phys.Lett. B614 (2005) 165–173, arXiv:hep-ph/0412116

[13] The ATLAS Collaboration, Eur. Phys. J C **72** 1849 (2012), doi 10.1140/epjc/s10052-011-1849-1